A theoretical framework for CV-QKD

Bodo Kaiser

December 14, 2021

Ludwig-Maximilians-Universität München & Huawei Munich Research Center

You never know what you might discover by thinking outside the box that culture, conformity, and critics have tried to impose. — T.D. Jakes

Outline

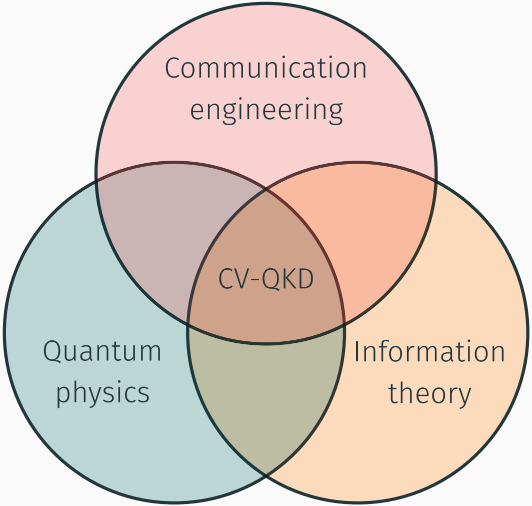

1. Introduction
2. Coherent state transmitter
3. Coherent state receiver
4. Conclusion and outlook

Introduction

Secure transmission system

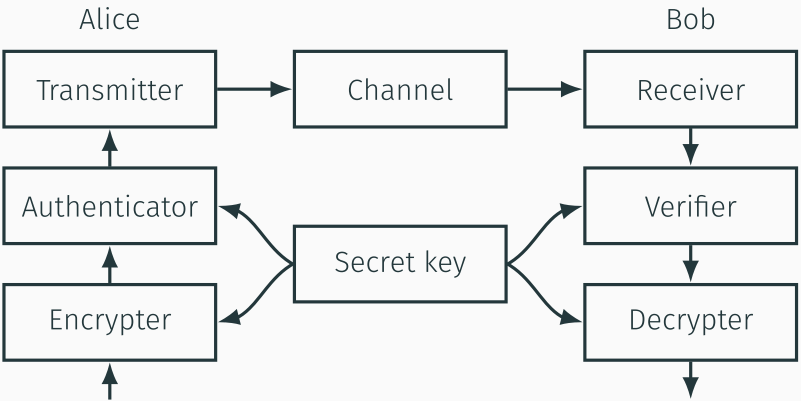

Figure 1: Block diagram of a secure transmission system.

Quantum key distribution system

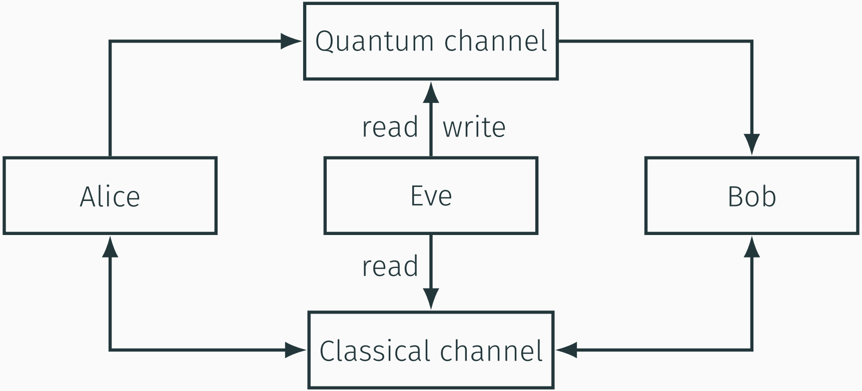

Figure 2: Block diagram of a quantum key distribution (QKD) system.

Table 1: Comparison of discrete- and continuous-variable QKD.

	Discrete	Continuous
Visualization	Bloch sphere	Phase space
Hilbert space (dim)	Finite (two)	Countable (infinite)
Observable	$\hat{\mathbf{S}}(\mathbf{n}) = \hat{S}_i n^i$	$\hat{X}(\vartheta) = \frac{1}{\sqrt{2}}\left(\hat{a}e^{-i\vartheta} + \hat{a}^\dagger e^{+i\vartheta}\right)$
Standard basis	$\{\lvert 0\rangle, \lvert 1\rangle\}$	$\{\lvert x\rangle, \lvert p\rangle\}_{x,p\in\mathbb{R}}$

Continuous-variable QKD using coherent states

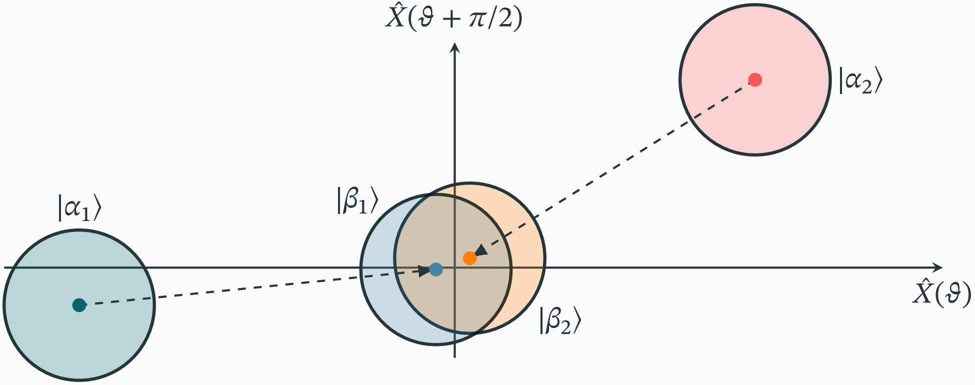

Figure 3: Phase space diagram of transmitted and received coherent states with mean (dots) and variances (opaque circles).

Continuous-variable QKD using continuous-time coherent states

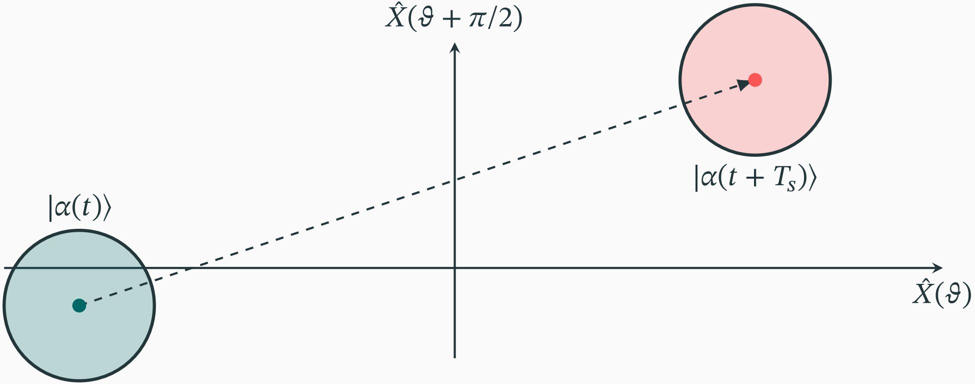

Figure 4: Phase space diagram of continuous-time coherent states with mean (dots) and variances (opaque circles) at two time instances.

Software-defined transmission system

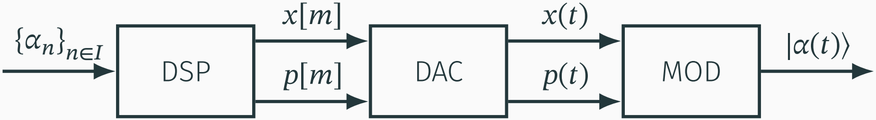

Figure 5: Block diagram of the software-defined transmitter architecture.

Figure 6: Block diagram of software-defined receiver architecture.

Coherent state transmitter

Digital signal processing pipeline for symbol encoding

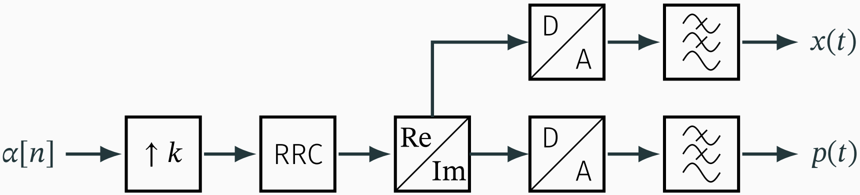

Figure 7: Block diagram of the digital signal processing for symbol encoding.

Symbol-encoding in the time domain

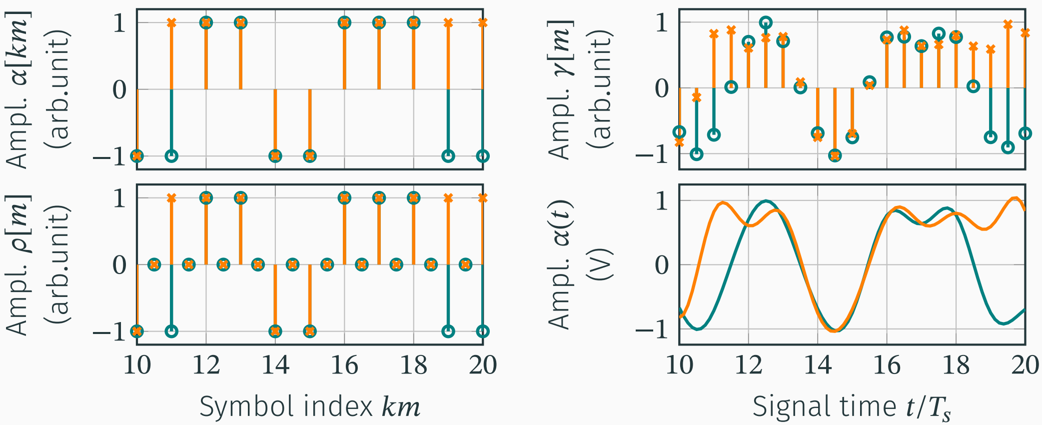

Figure 8: Symbol-encoding steps in the time domain for random QPSK sequence with real (orange) and imaginary (green) part.

Symbol-encoding steps in the frequency domain

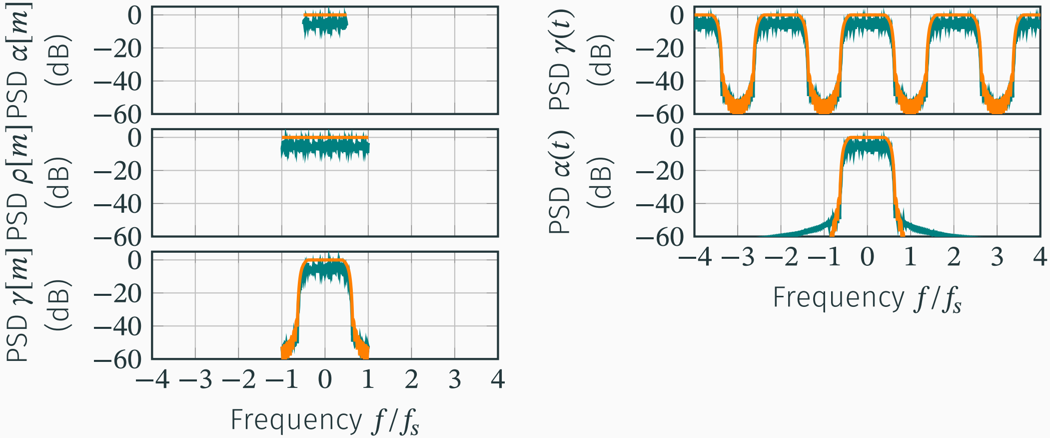

Figure 9: Symbol-encoding steps in the frequency domain for random symbols (green) and single symbol (orange).

Dual-quadrature upconversion in the time domain

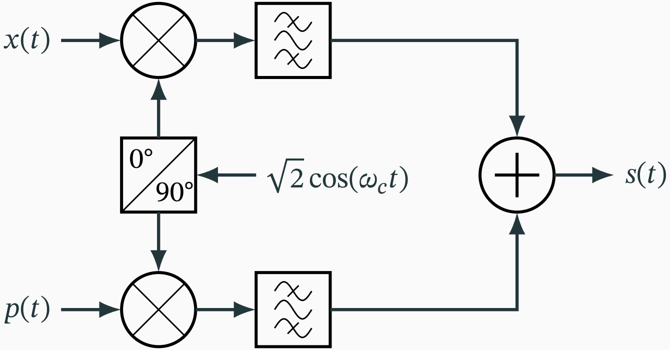

Figure 10: Power spectrum illustrating single-quadrature upconversion.

$$s(t) = x(t)\cos(\omega_c t) - p(t)\sin(\omega_c t) = \mathrm{Re}\left[\alpha(t)e^{+i\omega_c t}\right] \quad \text{with} \quad \alpha(t) = x(t) + i p(t) \tag{1}$$

Dual-quadrature upconversion in the frequency domain

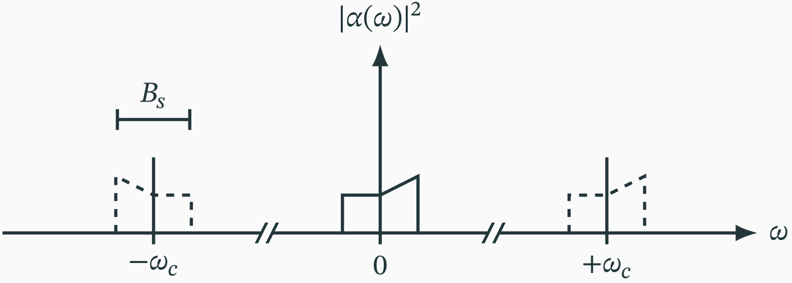

Figure 11: Power spectrum illustrating dual-quadrature upconversion.

$$s(t) = \mathrm{Re} \int_{\omega_0 - B_s/2}^{\omega_0 + B_s/2} \frac{\mathrm{d}\omega}{2\pi} \alpha(\omega - \omega_c) e^{+i\omega t} \tag{2}$$

In-phase and quadrature modulator as dual-quadrature upconverter

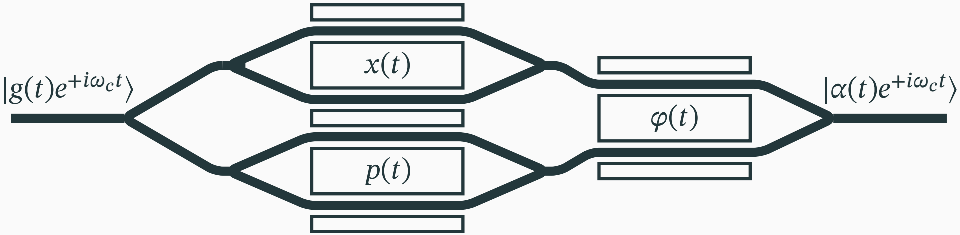

Figure 12: Drawing of an integrated in-phase and quadrature modulator.

$$|g(t)e^{+i\omega_c t}\rangle \rightarrow |\alpha(t)e^{+i\omega_c t}\rangle \qquad \alpha(t) = g(t)\,[x(t) + iq(t)] \tag{3}$$

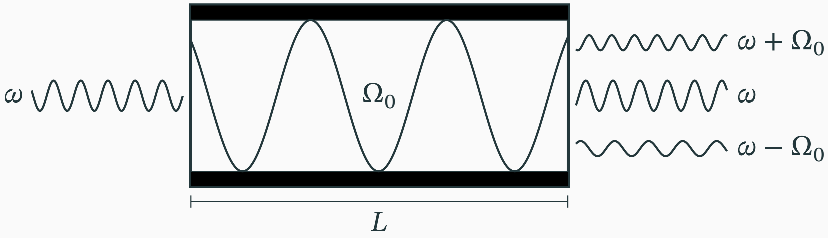

Figure 13: Traveling-wave electro-optical phase modulator of length L.

$$\hat{H}_{\text{int}} = \int \frac{\mathrm{d}\omega}{2\pi} \int \frac{\mathrm{d}\Omega}{2\pi} \mathrm{g}(\omega, \Omega) \hat{a}^{\dagger}(\omega) \hat{a}(\Omega) \hat{a}(\omega - \Omega) + \text{H.c.} \tag{4}$$

Single-mode frequency-conversion operator

Simplifying assumptions:

- $\hat{a}(\Omega) \to \beta(\Omega)$
- $\beta(\Omega) = \beta_0 2\pi\delta^{(1)}\delta^{(1)}(\Omega - \Omega_0)$
- $\theta e^{i\varphi}/2 = \beta_0^* g(\omega, \Omega)/T$

Evolution operator:

$$\hat{U}_{\text{int}} = e^{-\frac{1}{2}\theta \hat{T}_+(\Omega_0)e^{-i\varphi} + \text{H.c.}} \qquad (5)$$

Upconversion operator:

$$\hat{T}_+(\Omega_0) = \int \frac{\mathrm{d}\omega}{2\pi} \hat{a}^\dagger(\omega + \Omega_0)\hat{a}(\omega) \qquad (6)$$

$$[\hat{T}_+(\Omega_0), \hat{a}^\dagger(\omega)] = \hat{a}^\dagger(\omega + \Omega_0) \qquad (7)$$

Creation operator transform:

$$\hat{U}^\dagger \hat{a}(\omega)\hat{U} = \sum_{m\in\mathbb{Z}} J_m(\theta)\hat{a}(\omega + m\omega_l)e^{-im\vartheta} \qquad (8)$$

Coherent state receiver

Signal processing pipeline for symbol decoding

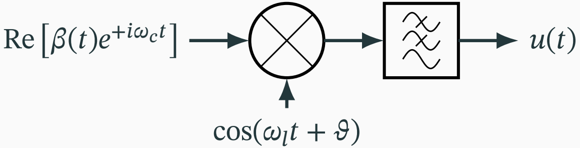

Figure 14: Block diagram of single-quadrature downconversion.

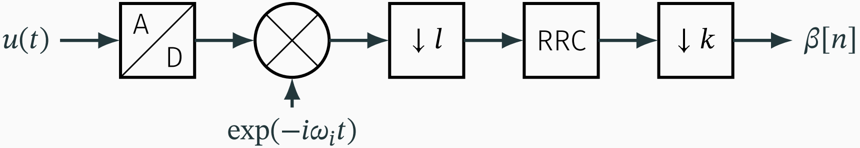

Figure 15: Block diagram of the analog-to-digital conversion and symbol-decoding.

Single-quadrature downconversion in the frequency domain

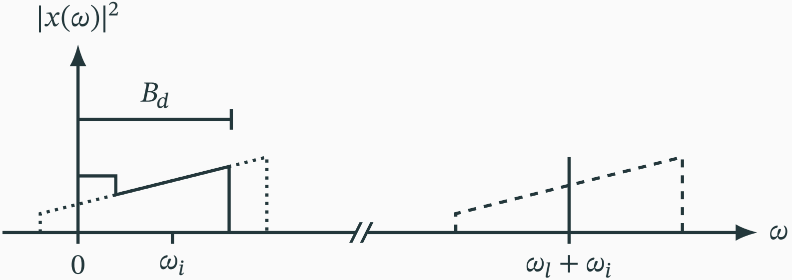

Figure 16: Power spectrum illustrating single-quadrature downconversion.

$$u(t) = \mathrm{Re} \int_0^{+B_d/2} \frac{\mathrm{d}\omega}{2\pi} \left[\beta(\omega + \omega_l) e^{+i\omega t} + \beta(\omega - \omega_l)^* e^{-i\omega t} \right] e^{-i\vartheta} \tag{9}$$

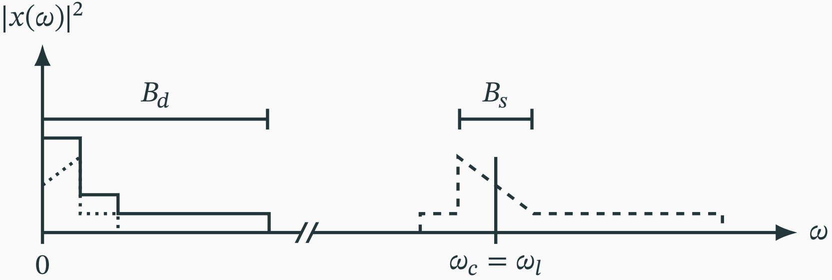

Figure 17: Power spectrum illustrating homodyne detection.

$$u(t) = \mathrm{Re} \int_0^{+B_d/2} \frac{\mathrm{d}\omega}{2\pi} \left[\beta(\omega) e^{+i\omega t} + \beta(\omega)^* e^{-i\omega t}\right] e^{-i\vartheta} \tag{10}$$

Single-quadrature heterodyne detection

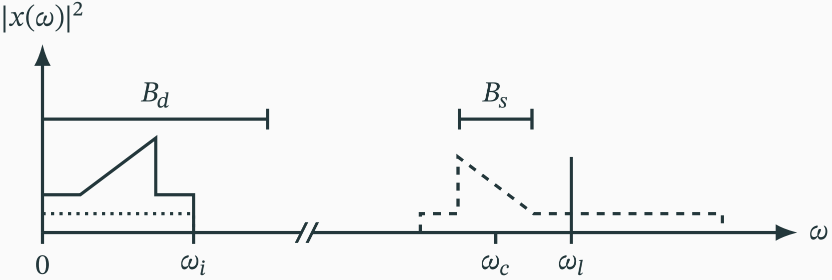

Figure 18: Power spectrum illustrating heterodyne detection.

$$u(t) = \mathrm{Re} \int_0^{+B_d/2} \frac{\mathrm{d}\omega}{2\pi} \left[\beta(\omega + \omega_i) e^{+i\omega t} + \beta(\omega - \omega_i)^* e^{-i\omega t} \right] e^{-i\vartheta} \tag{11}$$

Comparison homo- and heterodyne detection

Table 2: Comparison of coherent receiver designs and their implications

	Homodyne (single)	Homodyne (dual)	Heterodyne
Balanced detectors	1	2	1
Quadratures	1	2	2
Intermediate frequency	$\omega_i = 0$		$\omega_i \neq 0$
Optical complexity	Low	High	Low
Signal bandwidth	High	High	Low
LO synchronization	Frequency and phase	Frequency	Bandwidth
SNR	High	Low	Low

Balanced detector as single-quadrature downconverter

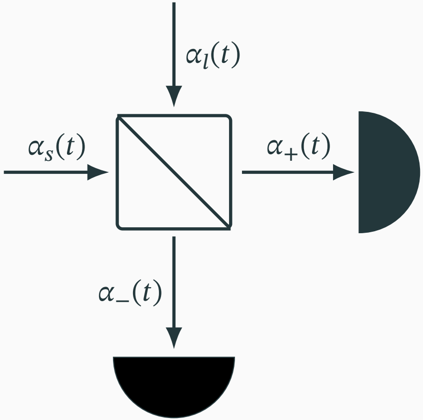

Figure 19: Electro-optical setup for balanced detection.

Differential photocurrent signal

$$i(t) \propto \mathrm{Re} \int_{-B_d/2}^{+B_d/2} \frac{\mathrm{d}\omega}{2\pi} \beta(\omega + \omega_l) e^{+i(\omega t + \vartheta)} \tag{12}$$

Phase-rotated quadrature operator

$$\hat{X}(t) = \int_{-\infty}^{+\infty} \frac{\mathrm{d}\omega}{2\pi} \left[\hat{a}(\omega) e^{-i(\omega t + \vartheta)} + \text{H.c.}\right] \tag{13}$$

Frequency-converted annihilation operator

$$\hat{U}^\dagger \hat{a}(\omega) \hat{U} = \sum_{m \in \mathbb{Z}} J_m(\theta) \hat{a}(\omega + m\omega_l) e^{-im\vartheta} \tag{14}$$

Conclusion and outlook

Summary

- Introduction to CV-QKD as a mechanism for secure key distribution.
- Raised awareness to dependence of transmissions.
- Introduction to a software-defined coherent transmission system.
- Introduction to concepts and methods from communication engineering.
- Extension of coherent transmission system to quantum regime.

Additional topics covered in the thesis

- Overview and comparison of DV- and CV-QKD protocols including post processing.
- Derivation of continuous-mode quantum theory of light rooted in quantum field theory.
- Summary of quantum models for the most important (electro-)optical components as building blocks for communication system.

Outlook

- Noise model for measurements.
- Comparison of image band and squeezing attack.
- Further transfer of telecommunication methods, e.g., orthogonal frequency-division multiplexing (OFDM).
- Properties of frequency-squeezed states.
- Equivalence of tensor-product with continuous-time coherent state transmission.

Maxwell equation of motion in the radiation gauge and momentum space

Free equation of motion in radiation gauge:

$$\partial_t^2 \mathbf{A} = \boldsymbol{\nabla}^2 \mathbf{A} \qquad A_0 = 0 \qquad \partial_i A^i = 0 \tag{15}$$

Four-dimensional Fourier transform:

$$\mathbf{A}(t, \mathbf{x}) = \int \frac{\mathrm{d}^4 p}{(2\pi)^4} \mathbf{A}(p_0, \mathbf{p}) e^{-ip_0 t + i\mathbf{p}\cdot\mathbf{x}} \tag{16}$$

Equation of motion in momentum space:

$$0 = (p_0 - \|\mathbf{p}\|)(p_0 + \|\mathbf{p}\|) \qquad \omega(\mathbf{p}) = \|\mathbf{p}\| \tag{17}$$

Plane-wave and polarization basis expansion in the radiation gauge

General plane-wave expansion in radiation gauge:

$$\begin{aligned}\mathbf{A}(t,\mathbf{x}) &= \int \frac{\mathrm{d}^4 p}{(2\pi)^3}\delta^{(1)}\left(p_0^2 - \omega(\mathbf{p})^2\right)\mathbf{A}(p_0,\mathbf{p})e^{-ip_0 t + i\mathbf{p}\cdot\mathbf{x}} \\ &= \int \frac{\mathrm{d}^4 p}{(2\pi)^3\sqrt{2\omega(\mathbf{p})}}\mathbf{A}(\omega(\mathbf{p}),\mathbf{p})\, e^{-ip_0 t + i\mathbf{p}\cdot\mathbf{x}} + \text{h.c.}\end{aligned} \tag{18}$$

Polarization basis expansion

$$\mathbf{A}(t,\mathbf{x}) = \sum_{\lambda=1,2} a_\lambda(\mathbf{p})\hat{\mathbf{e}}_\lambda(\mathbf{p}) \tag{19}$$

Polarization basis transverse to momentum:

$$\mathbf{p}\cdot\hat{\mathbf{e}}_\lambda(\mathbf{p}) = 0 \qquad \hat{\mathbf{e}}_\lambda(\mathbf{p})\hat{\mathbf{e}}_\sigma(\mathbf{p}) = \delta_{\lambda,\sigma} \qquad \sum_{\lambda=1,2}\hat{\mathbf{e}}_\lambda(\mathbf{p})^i\hat{\mathbf{e}}_\lambda(\mathbf{p})^j = \delta^{ij} - \frac{p^i p^j}{\mathbf{p}^2} \tag{20}$$

Canonical quantization in the Coulomb gauge

Conjugate momentum density:

$$\Pi_i = \partial_t A_i = E_i = -E^i \tag{21}$$

Equal-time commutation relations:

$$[\hat{A}_i(t,\mathbf{x}), \hat{E}_j(t,\mathbf{y})] = -i\delta^{(3)}_{\perp,ij}(\mathbf{x}-\mathbf{y}) \tag{22}$$

$$[\hat{A}_i(t,\mathbf{x}), \hat{A}_j(t,\mathbf{y})] = [\hat{E}_i(t,\mathbf{x}), \hat{E}_j(t,\mathbf{y})] = 0 \tag{23}$$

Transverse delta distribution:

$$\delta^{(3)}_{\perp,ij}(\mathbf{x}-\mathbf{y}) = \left(\delta_{ij} - \frac{\partial_i\partial_j}{\partial^2}\right)\delta^{(3)}(\mathbf{x}-\mathbf{y}) = \int \frac{\mathrm{d}^3 p}{(2\pi)^3}\left(\delta_{ij} - \frac{p_i p_j}{\mathbf{p}^2}\right)e^{i\mathbf{p}\cdot\mathbf{x}} \tag{24}$$

Maxwell field operators

Negative-frequency Maxwell field operator

$$\mathbf{A}^{(-)}(t,\mathbf{x}) = \sum_{\lambda=1,2} \int \frac{\mathrm{d}^3 p}{(2\pi)^3 \sqrt{2\omega(\mathbf{p})}} \hat{a}_\lambda(\mathbf{p}) \hat{\mathbf{e}}_\lambda(\mathbf{p}) e^{-i\omega(\mathbf{p})t + i\mathbf{p}\cdot\mathbf{x}} \tag{25}$$

Negative-frequency electric field operator

$$\mathbf{E}^{(-)}(t,\mathbf{x}) = -i \sum_{\lambda=1,2} \int \frac{\mathrm{d}^3 p}{(2\pi)^3 \sqrt{2\omega(\mathbf{p})}} \omega(\mathbf{p}) \hat{a}_\lambda(\mathbf{p}) \hat{\mathbf{e}}_\lambda(\mathbf{p}) e^{-i\omega(\mathbf{p})t + i\mathbf{p}\cdot\mathbf{x}} \tag{26}$$

Hamiltonian and momentum operator

$$\hat{H} = \sum_{\lambda=1,2} \int \frac{\mathrm{d}^3 p}{(2\pi)^3} \omega(\mathbf{p}) \hat{a}^\dagger_\lambda(\mathbf{p}) \hat{a}_\lambda(\mathbf{p}) \qquad \hat{\mathbf{P}} = \sum_{\lambda=1,2} \int \frac{\mathrm{d}^3 p}{(2\pi)^3} \mathbf{p} \hat{a}^\dagger_\lambda(\mathbf{p}) \hat{a}_\lambda(\mathbf{p}) \tag{27}$$

Axiomatic particle state construction

Vacuum state

Poincare invariance:

$$\hat{U}(a,\Lambda)|0\rangle = |0\rangle \tag{28}$$

Implies zero energy and momentum:

$$\hat{H}|0\rangle = 0|0\rangle \qquad \hat{\mathbf{P}}|0\rangle = \mathbf{0}|0\rangle \tag{29}$$

Implies annihilation operator destroying vacuum:

$$\hat{a}(\mathbf{p})|0\rangle = 0 \tag{30}$$

Momentum state

Algebraic commutation relations:

$$[\hat{N}, \hat{a}^\dagger(\mathbf{p})] = \hat{a}^\dagger(\mathbf{p}) \tag{31}$$

$$[\hat{\mathbf{P}}, \hat{a}^\dagger(\mathbf{p})] = \mathbf{p}\hat{a}^\dagger(\mathbf{p}) \tag{32}$$

Implies eigenstates:

$$\hat{N}\hat{a}^\dagger(\mathbf{p})|0\rangle = 1\hat{a}^\dagger(\mathbf{p})|0\rangle \tag{33}$$

$$\hat{\mathbf{P}}\hat{a}^\dagger(\mathbf{p})|0\rangle = \mathbf{p}\hat{a}^\dagger(\mathbf{p})|0\rangle \tag{34}$$

but not normalizable

$$\langle 0|\hat{a}(\mathbf{p})\hat{a}^\dagger(\mathbf{p})|0\rangle = (2\pi)^3\delta^{(3)}(\mathbf{p}-\mathbf{q}) \tag{35}$$

Smeared single-particle state

Interpretation as quantum operators as distributions:

$$\hat{A}^{(+)}[f]|0\rangle = \int \mathrm{d}^4x \, f(t, \mathbf{x})\hat{A}^{(+)}(t, \mathbf{x}) = \int \frac{\mathrm{d}^3p}{(2\pi)^3} \frac{f(\omega(\mathbf{p}), \mathbf{p})}{\sqrt{2\omega(\mathbf{p})}} \tag{36}$$

Normalizable iff:

$$\langle 0|\hat{A}^{(-)}[f]\hat{A}^{(+)}[f]|0\rangle = \int \frac{\mathrm{d}^3p}{(2\pi)^3} \left| \frac{f(\omega(\mathbf{p}), \mathbf{p})}{\sqrt{2\omega(\mathbf{p})}} \right|^2 = 1 \tag{37}$$

Implies eigenstates:

$$\hat{N}\hat{A}^{(+)}[f]|0\rangle = 1\hat{A}^{(+)}[f]|0\rangle \qquad \hat{H}\hat{A}^{(+)}[f]|0\rangle = \int \frac{\mathrm{d}^3p}{(2\pi)^3} \omega(\mathbf{p}) \left| \frac{f(\omega(\mathbf{p}), \mathbf{p})}{\sqrt{2\omega(\mathbf{p})}} \right|^2 \hat{A}^{(+)}[f]|0\rangle \tag{38}$$

Generalized number and coherent state

Number state

$$|n_f\rangle = \frac{1}{\sqrt{n!}}\hat{A}^{(+)}[f]^n|0\rangle \tag{39}$$

Mean energy:

$$n\int \frac{\mathrm{d}^3 p}{(2\pi)^3}\omega(\mathbf{p})\left|\frac{f(\omega(\mathbf{p}),\mathbf{p})}{\sqrt{2\omega(\mathbf{p})}}\right|^2 \tag{40}$$

Electric field at $(t,\mathbf{x})$:

$$0 \pm \frac{1}{2}\int \frac{\mathrm{d}^3 p}{(2\pi)^3}\omega(\mathbf{p}) + n|\Psi(t,\mathbf{x})|^2 \tag{41}$$

Coherent state

$$|\alpha\rangle = \exp\left\{\hat{A}^{(+)}[\alpha] - \text{H.c.}\right\}|0\rangle \tag{42}$$

Mean energy:

$$\int \frac{\mathrm{d}^3 p}{(2\pi)^3}\omega(\mathbf{p})\left|\frac{\alpha(\omega(\mathbf{p}),\mathbf{p})}{\sqrt{2\omega(\mathbf{p})}}\right|^2 \tag{43}$$

Electric field at $(t,\mathbf{x})$:

$$\int \frac{\mathrm{d}^3 p}{(2\pi)^3}\,\mathrm{Im}\left\{\alpha(\mathbf{p})e^{-i\omega(\mathbf{p})t+i\mathbf{p}\cdot\mathbf{x}}\right\} \pm \frac{1}{2}\int \frac{\mathrm{d}^3 p}{(2\pi)^3}\omega(\mathbf{p}) \tag{44}$$

Connection to continuous-mode quantum optics

Central assumption
No relative motion, i.e., no Lorentz boosts.

Typical approximations:

- Neglect polarization degrees of freedom
- Neglect transverse momentum distribution
- Neglect relativistic Lorentz factor $1/\sqrt{2\omega}$

Phase-rotated quadrature operator:

$$\hat{X}(t) = \frac{1}{\sqrt{2}} \int \frac{\mathrm{d}\omega}{2\pi} \left\{ \hat{a}(\omega) e^{-i(\omega t + \vartheta)} + \text{H.c.} \right\} \tag{45}$$

Maxwell field at $(t, \mathbf{x})$:

$$\hat{A}(t, \mathbf{x}) = \int \frac{\mathrm{d}\omega}{2\pi\sqrt{2\omega}} \left\{ \hat{a}(\omega) e^{-i\omega(t-x)} + \text{H.c.} \right\} \tag{46}$$